Bayesian Neural Networks for the Neutron Spectrum Unfolding in the EAST Tokamak

Baisong Zhou, Zhimeng Hu, Mingcai Zhong, Pin Gong, Guoqiang Zhong, Bin Shi, Jun Chen, Giuseppe Gorini, Massimo Nocente, Tieshuan Fan, and Xiaobin Tang

***Abstract*— Neutron spectra, as the key parameters of neutron fields around tokamaks, play a central role in evaluating the radiation harm to the staff and the ambient diagnostics for the normal operation of a tokamak. Several unfolding methods have been proposed for deriving neutron spectra from Bonner sphere spectrometer (BSS) counts. However, the main challenge in addressing this problem lies in the extreme sensitivity of the final solution to measurement data. The Bayesian neural network (BNN), which integrates knowledge-driven and data-driven merits, is suggested here to unfold the neutron spectra with a wide energy range and complex structure in the tokamak environment. In this study, a Monte Carlo model of Experimental Advanced Superconducting Tokamak (EAST) is constructed to generate the neutron spectra. The corresponding counts of BSS are also obtained using the experiment-evaluated response functions. These neutron spectra and BSS counts were used to train the BNN which could well predict the neutron spectra and their derived quantities, even when uncertainties of the BSS response functions are considered in the unfolding process. The comparison reveals that the BNNs outperform the other existing methods in terms of spectrum accuracy and robustness. Furthermore, verified by the BSS counts from two exposed positions collected during the EAST operations, this approach significantly enhances our ability to measure neutron energy spectra accurately.**

Received 22 August 2024; revised 24 October 2024; accepted 4 November 2024. Date of publication 24 March 2025; date of current version 9 April 2025. This work was supported in part by the National Natural Science Foundation of China under Grant 12375297 and Grant 12105144, in part by the International Research Cooperation Project of Jiangsu Province under Grant BZ2024018, and in part by the Primary Research and Development Plan of Jiangsu Province under Grant BE2022846. The Associate Editor coordinating the review process was Dr. Jing Lei. *(Corresponding author: Zhimeng Hu.)*

Baisong Zhou and Mingcai Zhong are with the Department of Nuclear Science and Technology, Nanjing University of Aeronautics and Astronautics, Nanjing 210016, China.

Zhimeng Hu, Pin Gong, and Xiaobin Tang are with the Department of Nuclear Science and Technology, Nanjing University of Aeronautics and Astronautics, Nanjing 210016, China, and also with the Key Laboratory of Nuclear Technology Application and Radiation Protection in Aerospace, Ministry of Industry and Information Technology, Nanjing University of Aeronautics and Astronautics, Nanjing 211106, China (e-mail: huzhm21@nuaa.edu.cn).

Guoqiang Zhong is with the Institute of Plasma Physics, Chinese Academy of Sciences, Hefei 230031, China.

Bin Shi and Jun Chen are with the National Key Laboratory for Metrology and Calibration Techniques, China Institute of Atomic Energy, Beijing 102413, China.

Giuseppe Gorini and Massimo Nocente are with the Department of Physics, University of Milano-Bicocca, 20126 Milan, Italy.

Tieshuan Fan is with the Institute of Plasma Physics, Chinese Academy of Sciences, Hefei 230031, China, and also with the School of Physics, Peking University, Beijing 100871, China.

Digital Object Identifier 10.1109/TIM.2025.3554325

***Index Terms*— Bayesian neural network (BNN), Bonner sphere spectrometer (BSS), spectra unfolding, tokamak.**

I. Introduction

IN TOKAMAK fusion devices like Experimental Advanced Superconducting Tokamak (EAST), neutron spectra, which are usually described as the energy distribution of fluence of the neutrons produced by fusion reactions, are particularly important as they are the input parameters for evaluating the radiation harm to staff and diagnostics, which are the essential issues for the normal operation of fusion devices [1], [2], [3]. In deuterium plasmas, these neutrons, primarily 2.45 MeV, interact with the tokamak structure and the surrounding environment in the EAST experimental hall, generating continuous neutron spectra that range from thermal energies to above 2.45 MeV. Significant efforts have been devoted to measuring the neutron spectra in fusion environments in order to benchmark the Monte Carlo simulation results, which might not be reliable due to the difficulties in the adequate description of the geometry and material components of numerical components of a tokamak and its surrounding equipment [2], [4], [5]. The Bonner sphere spectrometer (BSS) has a wide energy neutron response in the thermal-to- ∼MeV/GeV range, making it a good choice for the characterization of the neutron spectra around tokamaks. At EAST, two BSSs both, respectively, employing a ^{3}He proportional counter and a Diamond detector as the thermal neutron sensors have been developed for the neutron spectra measurement when the EAST works in low and high power operation [2], [5].

However, deriving accurate neutron spectra from BSS detector count rates presents a formidable challenge. This process, known as spectrum unfolding, is an ill-posed inverse problem [6]. The number of detectors (typically around 10) is significantly less than the number of energy bins required to adequately describe the wide-energy neutron spectrum. Consequently, the unfolding results are extremely sensitive to minor changes in the data, nonunique, and subject to significant uncertainty. Various approaches have been developed to address the challenge of neutron spectrum unfolding, which roughly fall into three categories: numerical analysis, intelligent heuristic, and neural network methods.

Numerical analysis approaches have specific and clear mathematical expressions, representing the most mature methods in this field. The predominant unfolding program is

the UMG developed by the Physikalisch-Technische Bundesanstalt (PTB), including GRAVEL and MAXED codes [7]. The good applicability of these codes has been widely verified for a long time [8]. They can produce reasonably good solutions provided the user chooses the appropriate initial spectrum. However, numerous sensitivity analyses of the codes have illustrated that it may also lead to inaccurate solutions if a priori information is diminished or if nonrealistic information is fed [9].

The second is the intelligent heuristic approach proposed by Freeman et al. [10], which performs well without spectral initialization. However, the occurrence of large oscillations in the unfolded spectra is not so easily resolved as it is still a challenge to design the appropriate spectrum-specific fitness functions or to set the suitable additional constraints [11]. Moreover, these two categories of methods generally necessitate iteration so they require users to have adequate experience with the code to manage input parameters and set appropriate stopping criteria effectively. This could be quite restrictive.

The third category, neural network methods, belongs to the data-driven techniques and are often referred to as closed box models. These methods rely solely on the counts as the input for prediction and can rapidly yield solutions [12]. However, the standard neural networks that only provide point estimates are demonstrated to be sensitive to training data, methodologies, and network architectures and are prone to overfitting issues [13]. In addition, they require sufficient data to train the model. Ortiz-Rodriguez et al. [14] revealed that neural networks with limited datasets suffer from sharp declines in generalization performance, potentially yielding wrong solutions. These limitations greatly restrict the applicability of this method.

The methods above are unable to effectively use the uncertainties inherent in the measurement process from the measurement data. This aspect is crucial for the BSS as the response functions often incorporate uncertainties in practical applications [15], [16]. In this respect, this article proposes an integration of knowledge-driven and data-driven strategies, the Bayesian neural network (BNN) method, for spectrum unfolding. The BNN's significant strength lies in its ability to handle noisy and small sample data, more importantly to resolve ill-inversed regression problems with uncertainty quantifications [17], [18] as the parameters are introduced into a probability distribution [19], [20], [21], [22], thereby effectively addressing posed by uncertain data that the above methods struggle to resolve [23]. These benefits have spurred our interest in applying BNNs to neutron spectra unfolding.

In this study, we demonstrate the capability of BNN for unfolding the BSS counts to derive the neutron spectra around a magnetic confinement fusion device when the BNN is trained only using the simulated neutron spectrum data which contain the characteristic structures of real neutron spectra. Initially, we developed an EAST Monte Carlo model to generate the required datasets and to achieve training BNNs through the elaborately designed structure. Subsequently, we evaluated the performance of the BNNs under conditions of both ideal and with uncertainties response functions and compared it with existing methods, including back-propagation neural network, genetic algorithm, and GRAVEL. Finally, we validated the reliability and benefits of the BNNs in practical applications by utilizing experimental data.

The main contributions of this article are as follows.

1) A method based on BNN has been developed for unfolding the neutron spectrum from BSS measurement data. The uncertainty of data is fully considered, resulting in a more efficient and reliable prediction.
2) The experimental validation of the BNN method using data from the EAST confirms its practical applicability and reliability for unfolding neutron spectra in the magnetic confinement fusion environment. This provides a fresh idea for improving the accuracy of the neutron spectrum unfolding in the other radiation fields.

The article is structured as follows. In Section II, the detector, the BNN model design, and data sources are presented. Section III discusses the simulated and experimental results, comparing the BNN method with traditional unfolding techniques. Section IV concludes with key findings and future research directions.

II. Method

A. Bonner Sphere Spectrometer

The BSS employs an SP9-type ^{3}He proportional counter provided by Centronic, U.K. [24]. The ^{3}He gas pressure, evaluated in the reference thermal neutron field [25] of the National Institute of Metrology, China, is 600 kPa, 13.9% lower than the nominal value. The sizes of the nine spherical moderators range from 2.5 to 12 in, with mass densities between 0.94 and 0.96 g/cm^3. More detailed parameters of the BSS model are thoroughly described in [15]. A total of 60 responses to monoenergetic neutrons were calculated using the MCNP6 code [26] with the combination of the F4 and FM4 tally cards. This includes the values at 21 energies from 1E-9 to 1E-2 MeV by 3 energies per decade, 33 energies from 1E-2 to 20 MeV by 10 energies per decade, and 6 experimental energies. A disk source with a diameter of 50 cm was defined to ensure full coverage of the largest Bonner sphere, which has a maximum moderator diameter of 12 in (30.48 cm). Each simulation involved 10^8 source neutrons to ensure statistical errors remained below 1%. Experimental evaluation of response functions was conducted in the neutron hall at Peking University, using the six monoenergetic neutron sources with energies of 0.144, 0.565, 1.2, 2.5, 5.0, and 14.0 MeV [16].

The response uncertainty of the BSS is attributed to the deviations from the real values for the ^{3}He gas pressure of the counter, moderator density, and air gap between the spherical moderator and the counter. In this study, we considered variations of $\pm 15\%$ in ^{3}He pressure, $\pm 2\%$ in moderator density, and an upper limit of 1.5 mm air gap variations [16]. Furthermore, statistical and experimental uncertainties associated with response calibration were also taken into account. A detailed analysis of the comprehensive influence of these factors on the response functions is presented in Section III-C.

B. BNN Model

The BNN method performs posterior inference by assigning probability distributions to neuron weight and bias parameters in a feed-forward neural network [26], defined as follows:

$$f(x,\theta) = a + \sum_{j=1}^{H} b_j \tanh\left(c_j + \sum_{i=1}^{I} d_{ij} x_i\right) \tag{1}$$

where $\theta = \{a, b_j, c_j, d_{ij}\}$ are the parameters of the model, $\{a, c_j\}$ are the biases, and $\{b_j, d_{ij}\}$ are the weights.

The inputs of the network are given by $x_i = \{C_1, C_2, \ldots, C_j\}$, which denotes the count of each sphere in the BSS. Since the choice of the activation function has in general a minor impact on the performance of a BNN, we assume a typically sigmoid, and the used tanh activation function, is defined as follows:

$$\tanh(t) = \frac{\exp(t) - \exp(-t)}{\exp(t) + \exp(-t)}. \tag{2}$$

The network predicts the fluence in each energy bin of neutron spectra, represented by a set of vectors $f(x_i, \theta) = \{\varphi_1, \varphi_2, \ldots, \varphi_n\}$.

The likelihood function $p(D|\theta)$ as a key hyperparameter and the objective function χ^2 are given by the following equation:

$$p(D|\theta) = \exp\left(-\chi^2/2\right)$$
$$\chi^2 = \sum_{l}^{N} \left[\varphi_l - f(x_i, \theta)\right]^2 / \Delta\varphi_l{}^2. \tag{3}$$

Equation (3) represents the cost function of the model which is set to be a Gaussian distribution, where $D = \{x_i^n, y_i^n\}_{n=1}^{N_d}$ denotes the sample data, N_d is the sample size and $\Delta\varphi_i$ denotes the corresponding noise level which is related to specific observables. The $\Delta\varphi_i$ in the likelihood function is another key hyperparameter. By the requirement that the standard deviation of the observation error is nonnegative, $\Delta\varphi_i$ is taken to be a half-normal distribution, rather than a fixed value in this work, allowing for introducing additional source of randomness and reducing model-dependent effects. The posterior distribution of the BNN can be obtained by appropriately generalizing Bayes' theorem

$$\underbrace{p(\theta|D)}_{\text{Bayesian Posterior}} = \frac{p(D_y|D_x,\theta)\,p(\theta)}{\int_\theta p(D_y|D_x,\theta')\,p(\theta')d\theta'} \propto \underbrace{p(D_y|D_x,\theta)}_{\text{Likelihood}} \underbrace{p(\theta)}_{\text{Prior}} \tag{4}$$

where $p(\theta)$ is artificially given a priori probability to network training, and the denominator term, also known as evidence, is the marginal distribution of the data, which is usually omitted as a normalization constant. Here, $p(\theta)$ is set to be a normal distribution. This treatment is routine, and helps to introduce a source of randomness in the training stage.

Due to the complexity of model parameters and nonlinearity, calculating the posterior probability directly can be challenging, especially with high-dimensional integrals. To address this issue, the Markov chain Monte Carlo (MCMC) method is employed for approximate computation. For a given new input x^*, the probability distribution of the predicted output distribution can be represented by the following equation:

$$p(y^*|x^*, D) = \int_\theta p(y^*|x^*, \theta)\, p(\theta|D) d\theta. \tag{5}$$

After sampling the posterior distribution, the predictive distribution for unobserved data is obtained through (5), which involves analytically intractable integrals. Therefore, Monte Carlo sampling methods are typically used for approximation by averaging over N_t samples from the posterior distribution for a given new input x_i

$$\widehat{y}_i = E\left[p(y^*|x^*, \mathcal{D})\right] = \frac{1}{N_t} \sum_{j=1}^{N_t} f(x_i, \theta_j). \tag{6}$$

In this work, due to the relatively limited amount of data, a significant consideration is the principle of statistical parsimony as a means of enhancing robustness. Consequently, only a single hidden layer has been considered in order to minimize the number of parameters that need to be estimated. The basic design steps for a BNN are outlined in Table I.

Here, the number of neurons in the hidden layer, the burn-in period, and the number of samples are treated as three key hyperparameters. The specific choice of the number of neurons is thoroughly analyzed in Section III-A. To guarantee the convergence of the Markov chain and the accuracy of the inferred posterior distribution, both the burn-in and sample sizes are set to 2000 in this study. The structure of the BNN model is shown in Fig. 1.

TABLE I
STEPS FOR DESIGNING THE BNN

Step	Design Choice
a) Structure of the BNN model	10 input features, 47 output features, a single hidden layer, neurons: Hyperparameters 1; tanh activation function for the first layer; linear activation function for the second layer
b) Prior distribution	Normal distribution (miu=0, sigma=1)
c) Likelihood function	Gaussian distribution (miu=φ, sigma=$\Delta\varphi$)
d) Noise level	Half-normal distribution (sigma=1)
e) Training inference method	Markov Chain Monte Carlo (MCMC)
f) Number of burn-in and posterior samples	Burn-in:Hyperparameters 2; Sample:Hyperparameters 3
g) Predictive probability distribution	Derived from posterior distribution using the expected values and confidence intervals

C. Training Dataset

A high-quality dataset is essential for training models. The IAEA (2001) report [27] only offers four fusion neutron spectra, which is insufficient for a comprehensive training set. To address this limitation, this study uses the MCNP code to calculate neutron spectra at different locations around the EAST hall, expanding the dataset. A model of the 45° sector of the EAST [5] was created, as shown in Fig. 2. This model's dimensions were derived from engineering documentation. It uses a mirror reflection design on the boundary to improve statistics efficiency and conserve computational resources. The input file of MCNP includes over 150 cells and more than 250 surfaces and contains all key parts of the tokamak, such as the superconducting toroidal field and poloidal field systems,

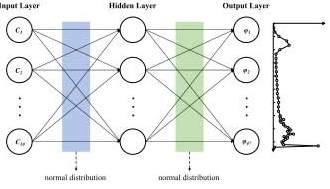

Fig. 1. Schematic for the BNN model with a single hidden layer used for neutron spectrum unfolding. The input layer consists of ten features, corresponding to the counts from ten detectors ($C_1, C_2, \ldots, C_{10}$). Each layer's weights and biases follow normal distributions, as indicated. The output layer provides the neutron spectrum at 47 discrete energy positions ($\varphi_1, \varphi_2, \ldots, \varphi_{47}$).

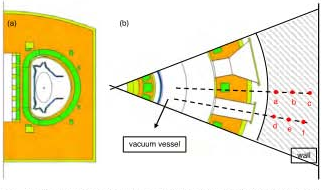

Fig. 2. Horizontal and vertical cross-sectional view of EAST at (a) vertical and (b) equatorial planes, respectively, obtained with MCNP (not to scale). The type of materials is indicated with different colors. Red dots indicate the locations corresponding to the six energy spectra used to validate the performance of the inverse method, as described in detail in Section III-B.

vacuum vessel, central solenoid, first wall, divertor, cryostat supports, ports, and experimental hall. In this model, the neutron source is approximated by monoenergetic neutrons (2.45 MeV), uniformly distributed within the plasma region inside the vacuum vessel. The 14 MeV neutrons produced from the secondary reaction of $D(T, n)\ ^4\mathrm{He}$ are reasonably disregarded due to their negligible contribution (<1%) to the overall neutron yield.

The neutron spectra in the MCNP model are divided into 47 energy bins, spanning 1E-9 to 3.16 MeV, with the same energy binning criterion as the response function. Neutron spectra were calculated using the F5 tally card of MCNP6 at various positions represented with shaded regions in Fig. 2(b). At each position, 10^8 source neutrons were used for each simulation to ensure statistical accuracy lower than 1%. To increase spectral diversity, rectangular cells simulating actual auxiliary systems (e.g., NBIs) were added to the original model. Multiple MCNP input files were generated by altering the model in this manner. For each input file, neutron spectra were calculated at an average of approximately 90 different positions, resulting in a total of 648 distinct spectra. This forms a dataset with dimensions of (47, 648), which serves as the output dataset for the BNN model.

Convoluting the well-calibrated response functions with each simulated neutron spectrum yields the corresponding count of each Bonner sphere using the formula below

$$C_j = \sum_{j=1}^{m} R_{ji}(E)\varphi_i(E), \quad j = 1, 2, \ldots, 10;\ i = 1, 2, \ldots, 47 \tag{7}$$

where C_j is the count of the jth sphere, $R_{ji}(E)$ is the response of the jth sphere to the ith neutron energy point, and $\varphi_i(E)$ is the fluence in the ith neutron energy point.

This computation yielded a (10, 648) array, serving as the input dataset for the BNN model.

D. Processing of Simulated Data

To prevent the model from favoring certain simulations, input and output data were scaled to a uniform range. For input (BSS counts), Z-score standardization was applied to achieve a mean of zero (μ) and unit variance (σ)

$$C_j' = \frac{C_j - \mu}{\sigma} \tag{8}$$

where C_j represents the raw data, μ and σ are the mean and standard deviation of the sample set, respectively. C_j' indicates the standardlized value.

For output (neutron spectra), two steps were applied: First, a logarithmic transformation was used to maintain nonnegativity and address multicollinearity. In order to guarantee the correct definition of the logarithmic processing, it is essential to set the flux to a minimal value of 1E-16 if the flux is 0. Therefore, the transformation applied is given by the following equation:

$$\varphi_i' = \log_{10}\left(\max\left(\varphi_i, 10^{-16}\right)\right). \tag{9}$$

Subsequently, min-max normalization was conducted to scale the transformed spectra to a specified range by the following equation:

$$\varphi_i'' = \frac{\varphi_i' - \varphi_{\min}'}{\left(\varphi_{\max}' - \varphi_{\min}'\right)} \tag{10}$$

where φ_i represents the raw data, $\varphi_{\max}'$ and $\varphi_{\min}'$ are the maximum and minimum datas. φ_i'' indicates the normalized value.

The neutron spectrum predictions with BNN approaches are then as follows:

$$\varphi_i^{\mathrm{pre}} = 10^{\varphi_i''} \tag{11}$$

where φ_i^{pre} represents the inversely normalized prediction from (11).

III. Results and Discussion

A. Optimization of the BNN Structure

The number of parameters in a BNN is key to the model's performance. To identify the optimal network structure, we evaluate different architectures and training strategies

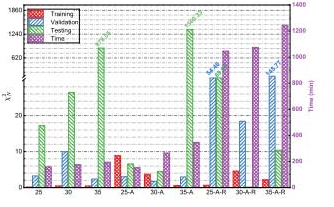

Fig. 3. Performance metrics of various BNN models with different architectures and training strategies. The ratio of training: validation: test datasets is 7:1.5:1.5. The horizontal axis denotes the number of neurons in the hidden layer, with "A" indicating data augmentation and "R" representing resampling.

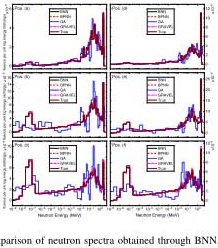

Fig. 4. Comparison of neutron spectra obtained through BNN, BPNN, GA, and GRAVEL methods at six distinct spatial positions, using ideal response functions of the BSS.

on 648 condition data. The training set was divided into a 70% training set for model training, a 15% validation set for model validation, and a 15% testing set for model testing. All the results were obtained using NumPyro on a CPU-based JAX platform [28]. The chi-square value $\chi^2_N = \sum_i [\varphi_i - f(x_i)]^2/N, (\times 10^{-12})$ and training time were selected as the primary evaluation metrics to derive the optimized BNN structure. By implementing a data augmentation and a resampling strategy, we presented the comparative results against the standard model in Fig. 3. It was indicated that more complex models are prone to local optima in the standard model. Furthermore, introducing a 5%–20% random error into the training set notably improved the training outcomes (except for BNN-35-A). However, attempts to apply reinforcement learning by resampling the points that had the top 2% of the largest deviations in the training set three cycles did not yield significant improvements. Contrary to expectations, this methodology resulted in a substantial increase in computational overhead.

In light of the analysis above, the BNN-30-A model (comprising 30 neurons and incorporating data augmentation) was ultimately selected as the optimal structure. This choice represents a reasonable balance between performance efficacy and computational efficiency.

B. Unfolding of Spectra Using the Ideal Response Functions

To evaluate the efficacy of the BNN method, we initially investigated the unfolding of an ideal response function. In this scenario, the response function uncertainty resources were disregarded. Six specific positions [denoted by red dots in Fig. 2(b)] were selected for analysis. Here, the initial energy spectra for GRAVEL were calculated at a distance of 1 m from the six positions.

Fig. 4(a)–(f) illustrates the unfolded spectra derived from the four methods. These spectra are characterized by distinct features: a deuterium-deuterium (DD) peak at 2.5 MeV, a high-energy peak spanning 0.01∼2.5 MeV, a flat region across a wide energy range (1E-7∼0.01 MeV), and a thermal peak within the energy range of 1E-9∼1E-7 MeV. Overall, the unfolded spectra obtained via the BNN, BPNN, and GRAVEL methods demonstrated good concordance with the true spectra. The GA method can reproduce in general the main structures of the spectra. However, significant oscillations around the true spectra occurred, especially at 0.1 MeV and within the thermal peak region.

To quantitatively assess the unfolding results, we employed the following criteria, namely, the root mean square error (RMSE) between the unfolded and true spectra, the relative deviations of three key parameters: total fluence rate ϕ, average energy $\overline{E}$, and neutron ambient dose equivalent rate $\dot{H}^*(10)$. In these quantitative criteria, RMSE directly measures the accuracy of the result, reflecting the quality of the unfolded spectrum; ϕ reflects the ability of the method to estimate the neutron intensity; $\overline{E}$ evaluates the energy distribution of spectrum, and to some extent indicates the neutron share of the different components; and $\dot{H}^*(10)$ validate the method's reliability in estimating radiation exposure risks. The calculation formulas are as follows, and the resultant data are presented in Fig. 5:

$$\mathrm{RMSE} = \sqrt{\frac{1}{n}\sum_{i=1}^{n}(\varphi_i - f(x_i, \theta))^2} \tag{12}$$

$$\phi = \sum_{i=1}^{n} \varphi_i(E_i) \tag{13}$$

$$\overline{E} = \frac{\sum_{i=1}^{n} E_i \times \varphi_i(E_i)}{\sum_{i=1}^{n} \varphi_i(E_i)} \tag{14}$$

$$\dot{H}^*(10) = \sum_{i=1}^{n} \varphi_i(E_i) \times h^*(E_i). \tag{15}$$

Fig. 5 indicates that the GRAVEL method performed well when employing an appropriate prior spectrum. It can be seen that there are only slight discrepancies between the unfolding results and the true spectrum. Specifically, a flat spectrum or nonfusion neutron spectra resulted in significant differences from the true neutron spectra at positions (a) and (c), as shown in Fig. 6. This highlights the GRAVEL method's sensitivity to initial conditions, potentially limiting its practical applicability when the spectrum information of a neutron field is not known. In the case of the BNN method, the distribution of the six positions in the boxplots appears to be somewhat inferior to

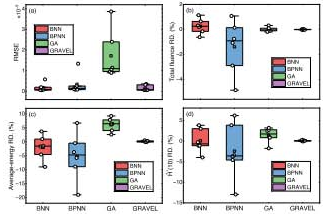

Fig. 5. Quantitative comparison of unfolding methods using ideal response functions. (a) RMSE, and relative deviations of (b) total fluence rate, (c) average energy, and (d) neutron ambient dose equivalent rate $\dot{H}^*(10)$. Each boxplot shows the distribution of values across the six positions, with the box indicating the interquartile range (IQR), the squares representing the average, the central line representing the median, and the whiskers extending to the minimum and maximum values within 1.5 times the IQR. Outliers are marked as individual points.

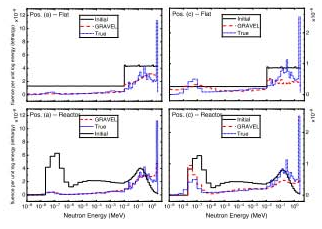

Fig. 6. Unfolded spectra of the GRAVEL method with varying initial energy spectra. The left column corresponds to position (a) in Fig. 2, right column to position (c). Detailed initial spectra are provided in the legend.

that of the GRAVEL method. However, in relative terms, the BNN method demonstrates good consistency concerning each criterion. This indicates the BNNs may have the potential to predict high-quality spectra with robust generalization ability. The BPNN method, despite exhibiting a lower RMSE, displayed a large distribution in the other three key metrics, reflecting poor stability. Regarding the GA method, despite the oscillations in the unfolded spectra around the target spectra leading to a higher RMSE, subsequent convolution with the fluence-to-dose equivalent conversion coefficient in calculating $\dot{H}^*(10)$ revealed that these oscillations had minimal impact on the reliability of dose estimation values.

C. Unfolding of Spectra Using the Response Functions With Uncertainties

Building upon the validation using ideal response functions, we further investigated the performance of the BNN method in the scenario when the real response functions of the BSS used in the unfolding process have deviations

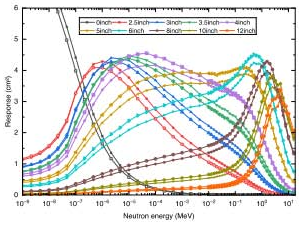

Fig. 7. BSS response functions calculated using MCNP. Curves with unfilled symbols represent the ideal response functions, while those with patterned filling indicate the response functions under the influence of three combined uncertainty factors.

from the ideal values, which lead to the difference of the BSS counts from the ideal conditions. For this investigation, we utilized the BNN model previously trained on the ideal response function dataset described in Section III-B. However, during the prediction phase, the uncertainty of the response function is taken into account. Therefore, we calculated a set of response functions incorporating a combination of maximum deviations contributed from those three factors mentioned in Section II-A to obtain the BSS counts to simulate the most challenging measurement scenarios. This "worst-case" analysis aimed to evaluate the BNN method's capacity to handle data with uncertainties and to determine its reliability in practical measurements through comparison with the other three selected methods.

Fig. 7 illustrates the resultant response function, where solid symbols represent the ideal response functions, and pattern-filled curves depict the discrepancy. Overall, the nine spheres combined uncertainty ranges from 6.8% to 14.3%, which was calculated using uncertainty propagation principles. Considering potential additional sources of uncertainty, we estimate the maximum uncertainty of the actual response function to be 15%.

After incorporating these uncertainties, we conducted a reevaluation of the spectrum unfolding results, which are presented in Fig. 8. In this scenario, the results from the GRAVEL method are highly influenced at positions (a) and (d) close to the tokamak, with unreasonable peaks emerging around 0.2 MeV. Fortunately, the influence is relatively minimal at the other positions. Despite the merit of stochastic optimization in the GA method, its results still showed a large discrepancy from the true spectrum. In contrast, the two neural networks seem to be less influenced, as their predicted results maintained good concordance with the true spectrum.

Fig. 9 illustrates the performance of each method for key parameters. Compared to the ideal response function scenario, all four methods exhibited different performance degradation. In terms of average energy and ambient dose equivalent rate $\dot{H}^*(10)$ indicators, BPNN and GA methods showed significant overestimation. The average relative deviation for BPNN's

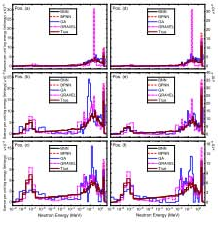

Fig. 8. Comparative analysis of neutron spectra obtained through BNN, BPNN, GA, and GRAVEL unfolding methods at six positions accounting for the three factors uncertainties: ±15% in ^{3}He pressure, ±2% in moderator density, and an upper limit of 1.5-mm air gap variations.

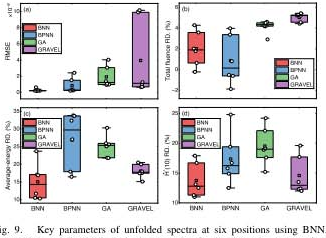

Fig. 9. Key parameters of unfolded spectra at six positions using BNN, BPNN, GA, and GRAVEL methods accounting for the above three uncertainty sources. (a) RMSE, (b) total fluence deviation, (c) average energy deviation, and (d) $\dot{H}^*(10)$ deviation.

average energy and $\dot{H}^*(10)$ increased from 7.3% to 27% and from 5.9% to 17.4%, respectively, with maximum values reaching 33.9% and 24.8%. Similarly, GA's values increased from 6% to 24.2% and from 2% to 19.6%, with maximum values of 30.5% and 24.1%, respectively. For GRAVEL, the overall results are satisfactory except for the two positions (a) and (d) resulting in larger RMSE.

Despite these challenges, the BNN method achieved the smallest RMSE among the four methods, with a mean total fluence rate deviation of 2%, average energy deviation of 14.7%, and $\dot{H}^*(10)$ deviation of 13.7%. Considering the maximum uncertainty of the response function, the results are highly exciting. This performance can be attributed to the capacity of BNNs to integrate uncertainty directly into the training process by probabilising the model parameters, which enables BNNs to more effectively address the uncertainty inherent in the data, leading to more precise and generalizable outcomes in terms of neutron spectrum. It is evident that traditional methods, such as GRAVEL, GA, and BPNN, are deficient in this regard, as they are incapable of accounting for uncertainties inherent in experimental measurements or response functions. Consequently, these methods frequently prove inadequate in providing reliable results when confronted with data containing uncertainty.

D. Unfolding of Experimental Data

To further evaluate the efficacy of the BNN method, we analyzed experimental data collected during EAST operations. These data are presented in Fig. 10. The detailed experimental procedure and data collection process are thoroughly described in [5].

Fig. 11(a) and (b) shows that the GA method failed to reflect structural characteristics in the unfolded spectra at both experimental positions, particularly at Position 2. The GRAVEL method exhibited unreasonable spectral characteristics in the high-energy region at Position 1, with a high peak around 0.1 MeV, and flux rapidly dropping to near zero with increasing energy, while the thermal peak shifted to the right. This phenomenon may be attributed to the fact

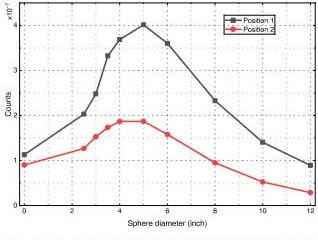

Fig. 10. Experimental measurement results of BSS count per source neutron.

that the initial spectrum may differ significantly from the true spectrum. Alternatively, overfitting may occur during the operation as a result of user input. In contrast, the spectra obtained using BNN and BPNN at both positions appeared more reasonable. However, in Fig. 11(c) and (d), the unfolded count rates from GA and GRAVEL showed better consistency with experimental values, within 4%, likely due to the use of the count rate as a constraint function in these methods. The BPNN method showed over 15% deviation in the count ratios for 2.5-, 10-, and 12-in spheres at Position 1 and 2.5-in sphere at Position 2, suggesting the necessity for further validation of the reliability of the predicted solution. Although the BNN method's unfolded count rates were slightly less accurate, the maximum deviations at both positions did not exceed 12% and 14%, remaining within acceptable limits.

In addition, Table II displays the fluence-averaged energy and $\dot{H}^*(10)$-mean energy at two exposed positions, showcasing a comparison between measured and calculated values. The measured values were determined using neutron spectra obtained through four different unfolding methods using the experimental data. The calculated values, which serve as a reference, were extracted from the [5]. It is important to note that the literature's initial spectra were computed using

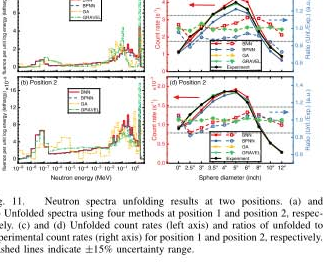

Fig. 11. Neutron spectra unfolding results at two positions. (a) and (b) Unfolded spectra using four methods at position 1 and position 2, respectively. (c) and (d) Unfolded count rates (left axis) and ratios of unfolded to experimental count rates (right axis) for position 1 and position 2, respectively. Dashed lines indicate ±15% uncertainty range.

TABLE II

COMPARISON OF MEASUREMENT AND CALCULATE VALUES FOR FLUENCE-AVERAGED ENERGY AND $\bar{H}^*(10)$-AVERAGED ENERGY AT TWO POSITIONS

		Measurement				Cal. [1]
Position 1		BNN	BPNN	GA	GRV. [2]	-
$\bar{E}$	Val. (MeV)	0.34	0.30	0.47	0.42	0.39
	C./M. (%)	1.15	1.30	0.83	0.93	–
$\bar{E}_{\bar{H}^*(10)}$	Val. (MeV)	0.87	0.84	1.59	0.43	1.08
	C./M. (%)	1.24	1.29	0.68	2.51	–
Position 2		BNN	BPNN	GA	GRV.	-
$\bar{E}$	Val. (MeV)	0.21	0.22	0.25	0.24	0.23
	C./M. (%)	1.10	1.05	0.92	0.96	
$\bar{E}_{\bar{H}^*(10)}$	Val. (MeV)	0.70	0.79	1.03	0.96	0.87
	C./M. (%)	1.24	1.10	0.84	0.91	–

MCNP at the two exposure positions, while this study was selected at a distance of 1 m from each one. The results in Table II reveal that employing the BNN method, the derived measurement values for average energy and $\bar{H}^*(10)$-mean energy were lower than their corresponding calculated values at both positions. However, the ratio between the calculated and experimental values demonstrated excellent consistency between the two positions. Conversely, despite the ratio of the other three methods being closer to 1 at Position 2, their results at Position 1 were unsatisfactory.

IV. SUMMARY AND CONCLUSION

In this study, we demonstrate the excellent performance of the BNN method for neutron spectrum unfolding in the EAST tokamak. Our analysis encompasses scenarios involving simulation data, which, respectively, use ideal response functions and the response functions with uncertainties mimicking the real conditions, as well as experimental data. By comparing the unfolded spectra and the derived quantities such as RMSE, total fluence rate, average fluence energy, and $\bar{H}^*(10)$, it is observed that while the other three methods effectively predict the neutron spectra in most instances, they remain inadequate when considering the uncertainties of BSS response functions. In contrast, the BNN method is able to well predict the neutron spectra in all three scenarios and appears to more accurately represent the values of various derived quantities, which are deemed entirely satisfactory. Experimental validation results indicated that although the values obtained from the BNNs slightly differed from the reference, the ratio between them exhibited better consistency at two exposed positions. This variance could be due to the utilization of simplified models and ideal response functions during network training.

In conclusion, thanks to the advantages of the BNNs combining knowledge-driven and data-driven merits, the unfolding of the neutron spectrum is no longer a purely mathematical problem or a fitting problem. Indeed, the BNN method suggests that it can efficiently overcome these difficulties caused by uncertainties. Future work will investigate the performance of the BNN method with other radiation fields, such as those from accelerator sources and nuclear power plant environments. In addition, we will explore incorporating a more comprehensive treatment of uncertainties into the unfolding process to enhance the stability and accuracy of the BNN method. These efforts can potentially serve the BNN method as a reliable and efficient tool for accurately unfolding neutron spectra in other radiation environments.

REFERENCES

[1] R. Juarez et al., "A full and heterogeneous model of the ITER tokamak for comprehensive nuclear analyses," *Nature Energy*, vol. 6, no. 2, pp. 150–157, Jan. 2021.

[2] Z. M. Hu et al., "An active bonner sphere spectrometer capable of intense neutron field measurement," *Appl. Phys. Lett.*, vol. 114, no. 23, Jun. 2019, Art. no. 233502.

[3] D. Stork et al., "Towards a programme of testing and qualification for structural and plasma-facing materials in 'fusion neutron' environments," *Nucl. Fusion*, vol. 57, no. 9, Sep. 2017, Art. no. 092013.

[4] R. Juárez et al., "Scoping studies of shielding to reduce the shutdown dose rates in the ITER ports," *Nucl. Fusion*, vol. 58, no. 7, Jul. 2018, Art. no. 076018.

[5] Z. Hu et al., "Neutron field measurement at the experimental advanced superconducting tokamak using a bonner sphere spectrometer," *Nucl. Instrum. Methods Phys. Res. A, Accel. Spectrom. Detect. Assoc. Equip.*, vol. 895, pp. 100–106, Jul. 2018.

[6] P. Panikkath, P. K. Sarkar, and S. Krishnaswamy, "A technique of solving an ill-posed inverse problem of neutron spectrum unfolding using a genetic algorithm search within Monte Carlo iterations," *Eur. Phys. J. Plus*, vol. 136, no. 4, p. 450, Apr. 2021.

[7] M. Reginato, B. Wiegel, A. Zimbal, and F. Langner, "Umg 3.3, analysis of data measured with spectrometers using unfolding techniques," PTB, Germany, Tech. Rep. NEA-1665, 2004.

[8] J. M. Gómez-Ros, R. Bedogni, C. Domingo, J. S. Eakins, N. Roberts, and R. J. Tanner, "Results of the EURADOS international comparison exercise on neutron spectra unfolding in bonner spheres spectrometry," *Radiat. Meas.*, vol. 153, Apr. 2022, Art. no. 106755.

[9] H. Mazrou, A. Nedjar, and T. Seguini, "Neutron spectrum measurements at a radial beam port of the NUR research reactor using a bonner spheres spectrometer," *Appl. Radiat. Isot.*, vol. 114, pp. 63–70, Aug. 2016.

[10] D. W. Freeman, D. Ray Edwards, and A. E. Bolon, "Genetic algorithms – a new technique for solving the neutron spectrum unfolding problem," *Nucl. Instrum. Methods Phys. Res. A, Accel. Spectrom. Detect. Assoc. Equip.*, vol. 425, no. 3, pp. 549–576, Apr. 1999.

[11] R. Li, J. Yang, X. Tuo, and R. Shi, "Research on fitness function of two evolution algorithms used for neutron spectrum unfolding," *J. Korean Phys. Soc.*, vol. 78, no. 2, pp. 109–115, Jan. 2021.

[12] Q. Zhu, G. Song, F. Song, Q. Guo, and Y. Wu, "Singular value decomposition and artificial neutral network for analyzing bonner sphere data," *Nucl. Instrum. Methods Phys. Res. A, Accel. Spectrom. Detect. Assoc. Equip.*, vol. 687, pp. 23–29, Sep. 2012.

[13] A. A. Alvar, M. R. Deevband, and M. Ashtiyani, "Neutron spectrum unfolding using radial basis function neural networks," *Appl. Radiat. Isot.*, vol. 129, pp. 35–41, Nov. 2017.

[14] J. M. Ortiz-Rodriguez et al., "A study using the robust design of artificial neural networks' methodology in neutron spectrometry," in *Proc. IEEE Int. Conf. Ind. Technol. (ICIT)*, 2016, pp. 1600–1606.
[15] Z. Hu et al., "Experimental determination of the response functions of a bonner sphere spectrometer to monoenergetic neutrons," *J. Instrum.*, vol. 12, no. 6, Jun. 2017, Art. no. T06002.
[16] Z. M. Hu et al., "Experimental evaluation of the Geant4-calculated response functions of a bonner sphere spectrometer on monoenergetic neutron sources," *Nucl. Instrum. Methods Phys. Res. A, Accel. Spectrom. Detect. Assoc. Equip.*, vol. 965, Jun. 2020, Art. no. 163836.
[17] Z.-A. Wang, J. Pei, Y. Liu, and Y. Qiang, "Bayesian evaluation of incomplete fission yields," *Phys. Rev. Lett.*, vol. 123, no. 12, Sep. 2019, Art. no. 122501.
[18] L. Neufcourt, Y. Cao, W. Nazarewicz, and F. Viens, "Bayesian approach to model-based extrapolation of nuclear observables," *Phys. Rev. C*, vol. 98, no. 3, Sep. 2018, Art. no. 034318.
[19] X. Zhang et al., "A novel Bayesian neural network approach for nuclear root-mean-square charge radii," *IEEE Trans. Nucl. Sci.*, vol. 72, no. 3, pp. 795–806, Mar. 2025.
[20] J. Tian, H. Song, G. Sheng, and X. Jiang, "Subsystem measurement-based condition assessment for power transformers via joint inference of data and knowledge," *IEEE Trans. Instrum. Meas.*, vol. 73, pp. 1–12, 2024.
[21] X. Han, X. Yang, S. Fung, R. Song, L. Li, and J. Zhang, "Noncontact blood pressure estimation using BP-related cardiovascular knowledge: An uncalibrated method based on consumer-level camera," *IEEE Trans. Instrum. Meas.*, vol. 72, pp. 1–13, 2023.
[22] R. Song, H. Wang, H. Xia, J. Cheng, C. Li, and X. Chen, "Uncertainty quantification for deep learning-based remote photoplethysmography," *IEEE Trans. Instrum. Meas.*, vol. 72, pp. 1–12, 2023.
[23] A. Kristiadi, M. Hein, and P. Hennig, "Being Bayesian, even just a bit, fixes overconfidence in relu networks," in *Proc. Int. Conf. Mach. Learn.*, 2020, pp. 5436–5446.
[24] *REM Counters*. Accessed: Aug. 10, 2024. [Online]. Available: http://www.centronic.co.uk/products/16/rem-counters
[25] P. Wang et al., "Thermal neutron reference radiation facility with high thermalization and large uniformity area," *Metrologia*, vol. 60, no. 4, Aug. 2023, Art. no. 045002.
[26] D. B. Pelowitz, "Mcnp6 user's manual version 1.0," Los Alamos Nat. Secur., Los Alamos, NM, USA, Tech. Rep. LA-CP-13-00634, 2013.
[27] *Compendium of Neutron Spectra and Detector Responses for Radiation Protection Purposes.*, Int. At. Energy Agency, Vienna, Austria, 2001.
[28] D. Phan, N. Pradhan, and M. Jankowiak, "Composable effects for flexible and accelerated probabilistic programming in NumPyro," 2019, *arXiv:1912.11554*.

Baisong Zhou is currently pursuing the M.Eng. degree in nuclear science and technology with the Department of Nuclear Science and Technology, Nanjing University of Aeronautics and Astronautics, Nanjing, China.

His research focuses on the study of unfolding methods for neutron spectra using a Bonner sphere spectrometer and the evaluation of the impact of response functions on neutron spectra under different factors.

Zhimeng Hu received the B.S. degree in nuclear physics and particle physics from Lanzhou University, Lanzhou, China, in 2012, and the Ph.D. degree in nuclear physics and particle physics from Peking University, Beijing, China, in 2017.

From 2017 to 2018, he was a Post-Doctoral Researcher with Peking University, and the University of Milano-Bicocca, Milan, Italy, from 2018 to 2021. He is currently an Associate Professor with the Department of Nuclear Science and Technology, Nanjing University of Aeronautics and Astronautics, Nanjing, China. His research interests include radiation detection methods and instruments and neutron measurements for fusion plasma diagnostics.

Mingcai Zhong is currently pursuing the M.Eng. degree in nuclear science and technology with the Department of Nuclear Science and Technology, Nanjing University of Aeronautics and Astronautics, Nanjing, China.

His research focuses on exploring the measurement methods for neutron ambient dose equivalent, designing neutron ambient dose equivalent meter, and evaluating the performance of the meter in different radiation fields.

Pin Gong received the B.Eng. degree in nuclear physics and nuclear technology from Nanjing University, Nanjing, China, in 2002, and the D.Eng. degree in nuclear technology and material engineering from Nanjing University of Aeronautics and Astronautics, Nanjing, in 2022.

He is currently an Associate Professor with the Department of Nuclear Science and Technology, Nanjing University of Aeronautics and Astronautics. His research interests include advanced particle detection and electronics.

Guoqiang Zhong received the B.Eng. degree in nuclear engineering and technology from the University of South China, Hengyang, China, in 2005, and the Ph.D. degree from the University of Science and Technology of China (USTC), Hefei, China, in 2018.

From 2005 to 2012, he was engaged in tokamak magnetic confinement fusion experimental research with the Institute of Plasma Physics, Chinese Academy of Sciences (ASIPP), Hefei, and is responsible for neutron and gamma-ray diagnostics. Since 2012, he has been mainly engaged in research related to fusion nuclear radiation monitoring and protection in ASIPP. He is currently an Associate Researcher with ASIPP.

Bin Shi, photograph and biography not available at the time of publication.

Jun Chen received the B.Sc. degree in solid physics from Jilin University, Jilin City, Jilin, China, in 1994, and the Ph.D. degree in radiation protection and environmental protection from China Institute of Atomic Energy (CIAE), Beijing, China, in 2015.

From 2004 to 2005, he was a Visiting Scholar with Japan Atomic Energy Research Institute, Tokai, Ibarakiken, Japan. He was a Researcher at CIAE, focusing on the areas of neutron metrology and micro-nano dosimetry.

Giuseppe Gorini received the dual B.S. degree (cum laude) in physics from Pisa University, Pisa, Italy, and Scuola Normale Superiore, Pisa, in 1985, and the Ph.D. degree (cum laude) in physics from Scuola Normale Superiore, in 1991.

For the past 30 years, he has been engaged in the development of new experimental methods for neutron measurements in fusion and material science. He is currently a Full Professor with the Department of Physics, University of Milano-Bicocca, Milan, Italy. His scientific production is documented in more than 800 journal articles.

Massimo Nocente received the master's (cum laude) and Ph.D. degrees in physics from the University of Milano-Bicocca, Milan, Italy, in 2008 and 2012, respectively.

He is currently an Associate Professor with the Department of Physics, University of Milano-Bicocca. His scientific production is documented in more than 200 journal articles. His main field of research is the development and application of nuclear instruments, particularly neutron and gamma-ray spectrometers, to study the physics of energetic particles in magnetically confined fusion plasmas.

Tieshuan Fan received the Ph.D. degree in nuclear physics from Peking University, Beijing, China, in 1994.

He is currently a Full Professor with Peking University. His main field of research is the physics of energetic particles in magnetically confined fusion plasmas, neutron detection techniques, asymmetric fission mechanism of intermediate-mass nuclei, and post-fission phenomena of actinide elements.

Xiaobin Tang received the B.Eng. degree in materials science and engineering and the D.Eng. degree in test metrology technologies and instruments from Nanjing University of Aeronautics and Astronautics, Nanjing, China, in 2000 and 2009, respectively.

He is currently a Full Professor with the Department of Nuclear Science and Technology, Nanjing University of Aeronautics and Astronautics. He published more than 200 research articles. His research interests include nuclear technology and applications mainly in medical physics, energy, space communication, and nuclear emergency.